IET Science, Measurement & Technology

Research Article

# Understanding the dielectric and mechanical properties of self-passivated Al–epoxy nanocomposites

ISSN 1751-8822
Received on 25th March 2019
Revised 3rd August 2019
Accepted on 10th September 2019
E-First on 3rd October 2019
doi: 10.1049/iet-smt.2019.0144
www.ietdl.org

*Naresh Chillu[1], Rengaswamy Jayaganthan[2], Michael G. Danikas[3], Toshikatsu Tanaka[4], Ramanujam Sarathi[1]* ✉

[1]*Department of Electrical Engineering, Indian Institute of Technology Madras, Chennai 600 036, India*
[2]*Department of Engineering Design, Indian Institute of Technology Madras, Chennai 600 036, India*
[3]*Department of Electrical and Computer Engineering, Democritus University of Thrace, 67100 Xanthi, Greece*
[4]*IPS Research Centre, Waseda University, Kitakyushu, Japan*
✉ *E-mail: rsarathi@iitm.ac.in*

**Abstract:** Epoxy nano passivated aluminium composites with optimised size and filler contents were fabricated. Variation in contact angle and surface roughness is insignificant with increasing filler into nanocomposites but it showed a drastic reduction on corona ageing. Water droplet initiated corona inception voltage (CIV) is high under the negative DC voltage followed with positive DC and AC voltages. The bandwidth of ultra-high frequency signal generated due to water droplet initiated corona discharge lies in the range of 0.5–1.2 GHz. Surface potential measurements have shown that the decay in the potential was fast initially, and it became slower and sluggish subsequently. The trap energy density versus trap depth plot exhibits shallow traps and deep traps at around 0.8 and 0.87 eV, respectively. Permittivity, conductivity and loss factor have increased with an increase in the filler content in nanocomposites. The bulk resistance and capacitance of samples were determined for obtaining the equivalent parallel RC circuit model. Incorporation of nanofillers increases the glass transition temperature and reduces the tan $\delta$ with increasing frequencies as evident from dynamic mechanical analysis studies. A direct correlation is observed between the plasma temperature measured through laser-induced breakdown spectroscopy spectra and hardness of the material.

## 1 Introduction

Recent studies have reported that the polymer nanocomposites with metallic additives (fillers) can serve as potential materials for electric energy storage capacitance materials, embedded capacitance materials and electromagnetic interference shielding materials in electronic circuits [1]. Also, these materials find their prominence as an insulating material for electric machines and power cable apparatus due to their ability to equalise the electric filed distribution during high-voltage stresses [2]. For all these applications, it is essential to choose a material with high dielectric constant, thermal conductivity, breakdown strength and low dielectric loss [3, 4]. Epoxy resin is widely used as the thermosetting polymer matrix in electrical, electronics and construction industries due to its good adhesive and filler dispersive properties. Polymer nanocomposites are the kind of materials that exhibit excellent thermal, mechanical and dielectric properties. They have the advantages of low cost, lightweight, ease of processing, increased modulus and strength, thermal stability, erosion resistance, good electrical insulation characteristics and high breakdown strength over the base material [5–7].

Nanocomposites with metallic filler exhibit high dielectric constant and electrical conductivity near the percolation threshold. Hence, intuitively, a material can be referred to as an insulator below the percolation threshold [8]. The percolation threshold of nanocomposite depends on filler size, shape and the specific gravity of filler and matrix. Addition of conductive fillers could improve the dielectric properties but suffer from poor thermal conductivity, breakdown strength, mechanical strength and dielectric loss, which restrict their use in capacitor applications [9]. Recent studies have shown that the controlled addition of self-passivated core–shell structured conductive filler to epoxy polymer matrix improves dielectric constant, electrical and thermal conductivity by maintaining relatively low dielectric loss over their base counterparts [6]. Core–shell structured self-passivated nanoparticles consist of Al metal spherical nanoparticles at the core surrounded by a few nm boundaries of aluminium oxide layer on the surface, which act as a shell [8, 10]. Usage of the self-passivated Al nanoparticles provides the uniform size distribution and helps to prevent oxidation for a longer period [11]. The addition of insulation shell to the surface of metal particle greatly influences the dielectric properties of the composite material.

Polymer nanocomposites with self-passivated metal particles have a layered structure with Al core at the first stage, the interface between core and polymer as the interfacial region at the second stage and polymer matrix as a third layer [6, 12]. The presence of Al particle at the core and interfacial region of the nanocomposites starts accumulating charges and increases the polarisability (alignment of dipoles) of the material under applied electric field [5, 6]. Thus, the increased interfacial polarisation increases the overall dielectric constant of the material. On the other hand, the oxide layer at the shell of nanocomposite obstructs the electron transfer among the neighbour metal particles and thereby decreases the dielectric loss [6].

With the establishment of mechanical and dielectric behaviour of polymer nanocomposites below the percolation threshold, further investigation is focused towards the utilisation of these materials as an insulation structure. The electrical breakdown and insulation characterisation of Al–epoxy nanocomposites at smaller filler size and concentration are scarce in the literature. The energy contained within the microsecond duration of the lightning surge is adequate enough to cause the catastrophic destruction to communication and power equipment with improper insulation structure. Inevitable surface discharge activity can happen when the insulation material is subjected to external electric field, upon exceeding certain limit the local electric field is enhanced due to accumulated electrons and ions inside the materials. Hence, it is essential to study the charge accumulation characteristics of a material under different voltage profiles [13–15]. Also, the water droplet on insulation material formed due to rain or fog condensation during power apparatus operation may lead to the formation of the corona and further leads to surface discharge activity due to enhancement in the local field. Sarathi *et al.* [16]

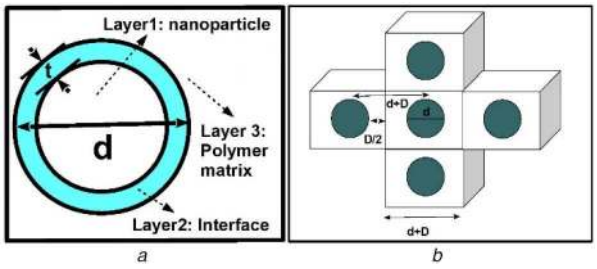


**Fig. 1** *Spherical nanoparticle having a*
***(a)*** Core–shell structure of epoxy nanocomposite, ***(b)*** Pictorial representation of spherical nanoparticle in a cubic lattice

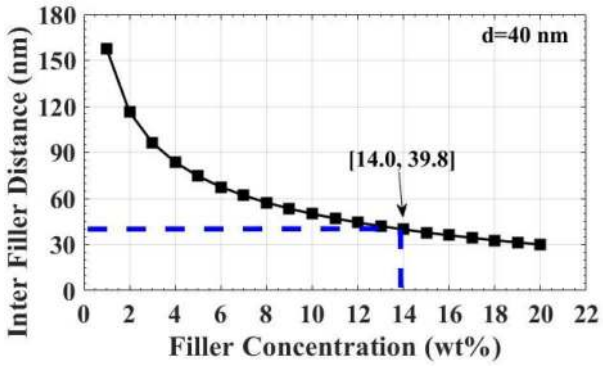


**Fig. 2** *Variation in inter-filler distance with respect to filler concentration*

have studied water droplet initiated corona discharges under different voltage profiles through radiated UHF signals. The discharges caused due to water droplet reduce the hydrophobicity of the material and formation of carbonised marking on the surface of the material, which further reduce the lifetime and cause the failure of insulation structure. Water droplet initiated discharges can cause major damage to the surface of the insulating material [17]. With the use of nanocomposite material, the level of damage due to water droplet initiated discharges under AC and DC voltages needs to be understood. The present study is focused towards the development of epoxy nanocomposites with the proper selection of fillers based on the percolation theory and subsequently, investigate their electrical and mechanical characteristics suitable for insulation structures. In specific, methodical experimental studies were carried out to understand the following important aspects: (i) experimental investigation on contact angle and surface roughness of virgin and corona-aged Al–epoxy nanocomposites, (ii) variation in corona inception voltage (CIV) due to water droplet under AC and DC profile voltages, (iii) the surface charge and trap characteristics under DC voltage and lightning impulse voltage profiles, (iv) experimental studies to understand the variation in dielectric properties and modelling of Al–epoxy nanocomposites, (v) the characteristic variation in mechanical properties over the different filler grades through dynamic mechanical analysis (DMA) studies and (vi) ranking the performance of Al–epoxy nanocomposites through laser-induced breakdown spectroscopy (LIBS) technique.

## 2 Experimental studies

### *2.1 Selection of filler size and optimised weight fraction*

It is well known that the filler of smaller sizes with percolation threshold provides high surface area for reactivity and hence improves the dielectric properties. The core–shell structure of filler was assumed for the theoretical calculation of percolation threshold [12]. Fig. 1*a* shows the typical core–shell structure of a nanoparticle in a nanocomposite with Al core, interfacial phase of thickness $t$ and polymer matrix at the third phase. The volume fraction of interfacial area is the ratio of volume of interfacial region to volume of particle with diameter $d$ [12].

It is found that the nanoparticle of 40 nm with an interface thickness of 2 and 4 nm occupies 27 and 50% of the total volume, respectively. It is clear that the small interfacial region over the core of nanoparticle has huge impact on electrical characteristics over its pure metal and base counterparts [18]. Hence, for the present study, Al nanoparticles with average particle size of 40 nm and passivation coating extended up to 2–4 nm were chosen. When the core–shell structure of the spherical nanoparticle with diameter $d$ is dispersed in a cubical lattice of the polymer matrix as shown in Fig. 1*b*, it is believed that the maximum amount of uniform dispersion is possible provided the inter-filler distance $D$ is equal to the diameter of the nanoparticle $d$ [12]. For the structure shown in Fig. 1*b*, theoretically, the inter-filler distance can be calculated from the following expression [12]:

$$D = \left\langle \left\{ \frac{\pi}{6}\left(\frac{\rho_n}{\rho_m}\right)\frac{100}{\text{wt\%}}\left[1 - \frac{\text{wt\%}}{100}\left(1 - \frac{\rho_m}{\rho_n}\right)\right]\right\}^{1/3} - 1 \right\rangle * d \quad (1)$$

where $\rho_n$ and $\rho_m$ are the specific gravities of Al nanofiller and the polymer matrix ($\rho_m = 1.17$ and $\rho_n = 2.7$), respectively. Fig. 2 shows the variation of inter-filler distance over different filler weight percentages.

It can be observed from Fig. 2 that the higher filler concentration entails the reduced inter-filler distance which eventually leads to agglomeration, whereas for the lower filler content shows the case of uneven dispersion due to higher inter-filler distance. Hence, the optimum filler loading can be chosen at 14wt%, where the inter-filler distance (39.8 nm) and particle diameter (40 nm) are almost equal. Hence, for the present study, the theoretical percolation threshold was chosen at 14 wt% and below this value, the material is presumed to act as an insulator. With the theoretical threshold estimated, the samples were prepared with filler concentrations of 0, 0.5, 1, 2, 5, 10 and 14 wt% in the present work.

### *2.2 Materials and method of sample preparation*

Materials used in preparing the nanocomposites consist of bisphenol-A epoxy resin (CY205) as a base polymer matrix, ethanol as a solvent, tri ethylene tetra amine (TETA) hardener as a curing agent and self-passivated spherical aluminium nanoparticles of 99.9% purity with an average particle size of 40 nm (supplied by Hongwu International Group Ltd., Hong Kong). At the first stage, the required quantity of nanopowder was preheated at 110°C for 12 h to remove excess moisture content. Also, the required quantity of epoxy resin was taken in another beaker and kept in a vacuum desiccator for 1 h to remove trapped air bubbles. The preheated nanopowder mixed with ethanol for 1 h. Ethanol and nanofiller mixture was mixed with epoxy in a controlled shear mixing at a rotating speed of 2000 rpm for 6 h. After that, the high-frequency sonication process (at 20 kHz) was carried out by keeping the sample temperature at 40°C by using an ice-filled water bath, for 2 h. Prior to the addition of hardener for curing, the mixture was kept in an oven for allowing the excess ethanol to evaporate from the mixture. A required quantity of hardener was added to the nanoparticle dispersed epoxy mixture and mixed thoroughly till the uniform dispersion was achieved. Upon degassing, the mixture was cast into the desired size for various tests.

### *2.3 Electrical characterisation*

*2.3.1 Contact angle and surface roughness:* Corona ageing causes the dissociation of polymer chains and modifies the surface structure of the material [17, 19, 20]. Hence, the samples were subjected to artificial corona ageing treatment for 10 min to find the variation in hydrophobicity. Static contact angle measurement was employed to find the hydrophobicity of the sample surface. Here, the set of samples with corona-aged treatment is referred as aged sample, whereas the samples without ageing referred as virgin samples. About 20 µl deionised water drop was used as droplet for static contact angle measurement of virgin and aged samples. The static contact angle ($\theta$) was measured through the following equation:

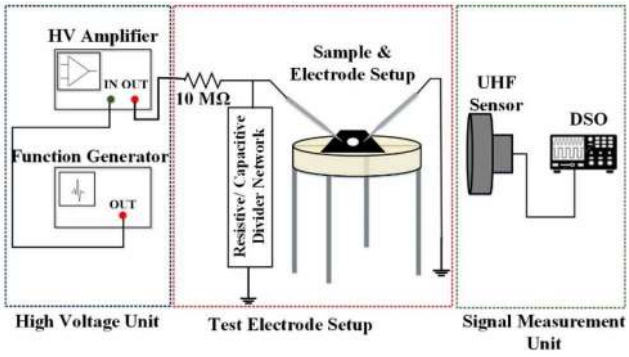


**Fig. 3** *Experimental setup for water droplet initiated discharges*

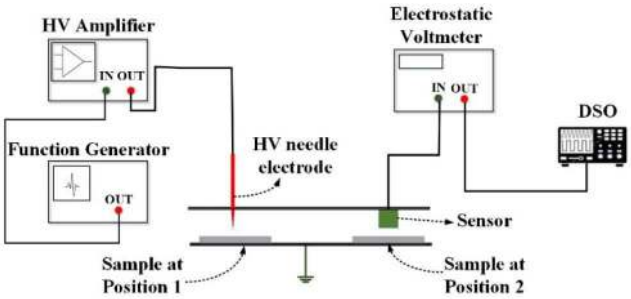


**Fig. 4** *Experimental setup for surface potential decay studies*

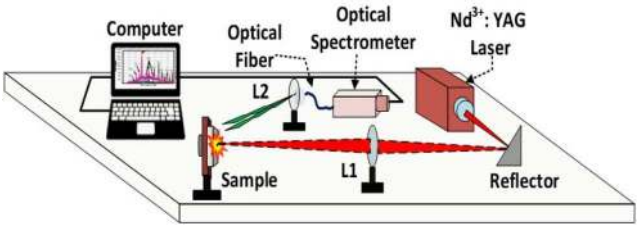


**Fig. 5** *Experimental setup for laser-induced breakdown spectroscopy*

$$\theta = 2 * \tan^{-1}\left(\frac{2h}{d}\right) \quad (2)$$

where $d$ and $h$ are the diameter and height of the liquid drop on the sample surface. Readings were taken at six different locations and averaged. Surface roughness was measured through surface profilometer and measured for both virgin and aged samples to understand the effect of corona ageing on the surface structure of samples.

*2.3.2 Water droplet initiated discharge:* Water droplet initiated surface discharge on Al–epoxy nanocomposite was measured using the experimental setup for AC and DC voltages, as per IEC 60 112, shown in Fig. 3.

It mainly consists of (i) a high-voltage unit, (ii) a test electrode setup and (iii) a signal measurement unit. AC/DC voltage is generated through Trek amplifier (Model 20/20C), with input from a function generator (Agilent 33250A). The high-voltage source and the test electrode are connected through current limiting resistor and the other electrode is connected to the ground. The electrodes were separated by 10 mm on a 1.5 mm thickness sample. Standard 20 µl deionised water was used for discharge studies. The UHF sensor used in the present study is basically a non-directional UHF sensor. The sensor was kept at a distance of 20 cm from the test electrode setup to acquire radiated signals due to water droplet initiated discharges. Signals acquired by the UHF sensor were acquired through digital storage oscilloscope (DSO) (Lecroy WavePro 7300A, 3.5 GHz, sampling rate 20 GSa/s).

*2.3.3 Surface potential measurements:* Needle plane configuration depicted in Fig. 4 was used to investigate the charge transportation behaviour through surface potential decay characteristics. The needle plane electrode connected to a high-voltage source injects the charges over the sample, which was located at position 1 for 3 min. After 3 min, the sample was shifted to position 2 where the potential remains on the surface was measured under isothermal conditions through an electrostatic voltmeter (Trek model 341B) and subsequently data was captured through the DSO. Readings were taken for 4 times per sample and averaged. In this study, the surface potential decay characteristics were observed for 8 kV DC voltage and 8 kV lightning impulse signal.

*2.3.4 Dielectric relaxation spectroscopy (DRS):* The DRS analysis of the nanocomposite was carried out through broadband dielectric/impedance spectroscopy analyser (Novocontrol technologies) for understanding the variation of dielectric constant ($\epsilon$), conductivity ($\sigma$) and dielectric loss ($\tan\delta$) of the sample over wide frequency range from 0.01 Hz to 10 MHz, at room temperature. Samples for testing were cut into a circular disc (20 mm diameter and 1.5 mm thickness).

### *2.4 Mechanical characterisation*

Vickers hardness test was carried out at room temperature by applying a load of 0.98 N for 15 s on the samples at six different positions through Wolpert Wilson Instruments (Model: 402MVD) to find the surface hardness of samples. To understand the viscoelastic behaviour of the nanocomposites, DMA was carried out under controlled sinusoidal strain over a temperature range from 25 to 200°C and at different frequencies (1, 10, 25 and 50 Hz). The experiments were performed on samples cut into a rectangular shape with 55 mm × 11.5 mm dimension, with an incremental heating rate of 2.5°C/min, under the flow of liquid nitrogen.

### *2.5 Laser-induced breakdown spectroscopy*

LIBS setup was used for elemental analysis and quantification. When the sample is subjected under high-energy and short-pulsed laser, the material surface gets ablated and the plasma plume forms due to intense heating and ionisation. The emitted radiation from the plasma is spectrally resolved and used as a fingerprint for elemental identification and quantification of ablated material. The pictorial representation of LIBS experimental setup is shown in Fig. 5. The laser beam from $Nd^{3+}$:YAG laser source was allowed to shine the sample through the focusing lens L1 with the focal length of 25 cm. Emission from the plasma due to laser shine was captured through the capture lens L2 having the focal length of 100 cm. Optical spectrometer (Ocean Optics) was employed to measure the peak intensities versus wavelengths through multimode optical fibre with core diameter of 400 µm and 0.22 numerical aperture. One second integration period was used to get the spectra.

## 3 Results and discussion

### *3.1 Electrical properties of epoxy nanocomposite*

*3.1.1 Contact angle and surface roughness measurement:* The variation in the surface roughness and contact angle of epoxy nanocomposites before and after corona ageing is shown in Fig. 6. It is observed that the contact angle and surface roughness are practically the same for virgin epoxy–aluminium nanocomposites, irrespective of filler concentration. On corona ageing, a drastic reduction in the contact angle and increased surface roughness of the material were observed. This clearly indicates that the surface roughness and the contact angle have an inverse correlation.

Also, it is observed that with nanocomposites, the contact angle is relatively high with nanocomposites up to 2 wt% of nanoaluminium included, above which a marginal reduction is observed. The water droplet sitting on the sample was strongly attached to the surface and the increment in surface energy due to corona ageing eventually led to a reduction in the contact angle and thereby decrement in the hydrophobic nature of the material is

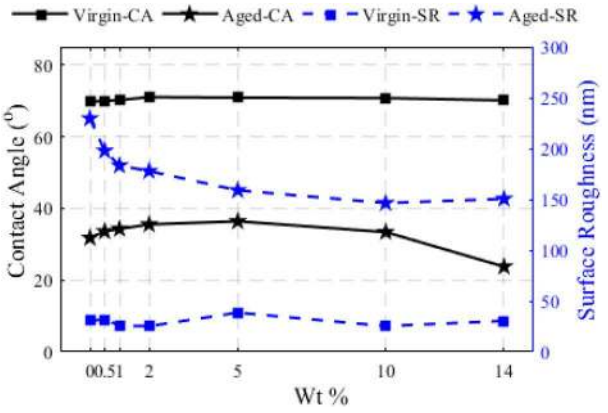


**Fig. 6** *Variation in the contact angle and surface roughness of virgin and corona-aged epoxy nanocomposites*

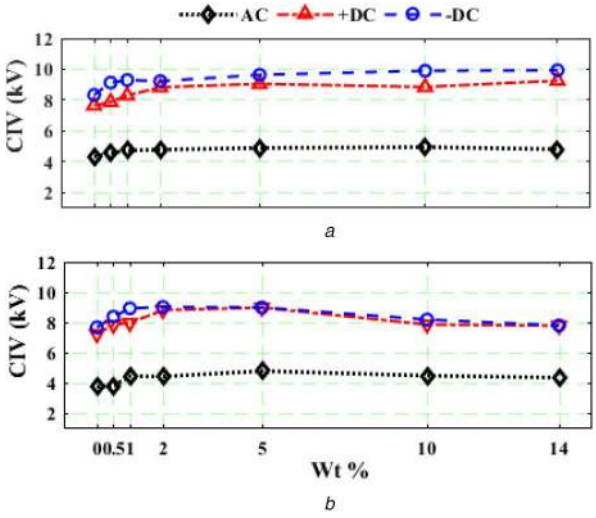


**Fig. 7** *Variation in water droplet initiated CIV in* ***(a)*** Virgin, ***(b)*** Corona-aged epoxy nanocomposites

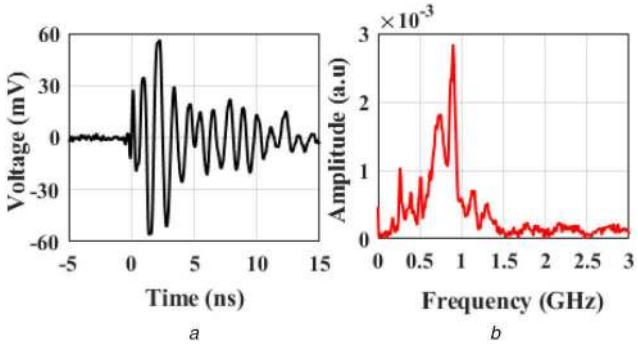


**Fig. 8** *Water droplet initiated CIV with* ***(a)*** Typical UHF signal detected at the instant of discharge, ***(b)*** Its corresponding FFT

observed [20]. Similarly, the surface roughness has reduced with increasing weight percentage of nanofiller in epoxy nanocomposites. This indicates a strong interfacial bonding between the filler and matrix which enables the material to modify its surface structure slightly at higher filler concentrations, whereas it is excessive at lower concentrations. Significant improvement in the contact angle can be observed up to 10 wt% for corona-aged samples and beyond which it is reduced again. The corona ageing causes the alteration in surface energy and surface roughness which could be the possible reasons for reduction in the contact angle for corona-aged samples.

*3.1.2 Water droplet initiated discharge studies:* The variation in water droplet initiated CIV with epoxy nanocomposites under AC and DC voltages is shown in Fig. 7.

The voltage at which UHF sensor generates UHF signal, on the application of voltage, is defined as CIV [16, 20]. It is observed from Fig. 7 that from 0 to 5 wt%, CIV increases slightly. On the other hand, between 5 and 14 wt%, CIV decreases slightly. For corona-aged specimen, CIV decreases slightly after treatment over their virgin counterparts. The cause for variation in CIV is due to the contact angle or surface roughness of the material as well as water droplet movement on application of voltage [17]. In general, the contact angle (Fig. 6) and CIV (Fig. 7) of the material exhibit a direct correlation.

The typical UHF signal generated due to water droplet situated on epoxy nanocomposites, on the application of voltage is shown in Fig. 8*a*, and its corresponding fast fourier transform (FFT) analysis is shown in Fig. 8*b*. The results indicate that the bandwidth of the signal lies in the range of 0.5–1.2 GHz.

*3.1.3 Surface potential decay characteristics under DC voltage:* The potential decay characteristics of Al epoxy nanocomposites as a function of filler concentration under the DC corona activity are shown in Fig. 9. The potential decay behaviour on the removal of charge injection from the corona electrode can be quantified as

$$U(t) = U_0 * \mathrm{e}^{-\lambda * t} \tag{3}$$

where $U_0$ is the initial potential and $\lambda$ is the decay rate constant. The mean lifetime can be defined as $\tau = 1/\lambda$.

Table 1 shows the mean lifetime of samples under positive and negative DC corona activities. Although the impurities in the material act as trapping sites for transported charges, the thermal agitation due to the collision of charges allows them to detrap and prolong their transportation towards the ground electrode and eventually leads to decay in the potential. Studies have indicated that the initial fast potential decay is credited to detraping of charges from shallow traps and the subsequent slower potential decay is ascribed to detraping from deep traps [15].

The density of trapped charges ($N(E)$) at different energy levels ($E$) follows the decay behaviour within the bulk of the material with the variation of trap depth ($\Delta E$) [13], i.e.

$$N(E)\alpha t * \frac{\mathrm{d}U}{\mathrm{d}t} \tag{4}$$

and trap depth

$$\Delta E = E_\mathrm{c} - E_\mathrm{d} = kT * \ln(vt) \tag{5}$$

where $E_\mathrm{c}$ is the bottom of the transport state and $E_\mathrm{d}$ is the demarcation energy level which separates the emptied and occupied states and $v$ is the attempt frequency, in the order of $10^{12}$ $\mathrm{s}^{-1}$.

The variation in trap energy density with respect to different energy levels is shown in Figs. 10*a* and *b* for the nanocomposites with the different filler contents under DC corona activity. It is observed that the trap distribution covers the range from 0.75 to 0.95 eV. The trap depth at maximum energy density is treated as a trap centre [14]. It is observed that the samples with filler loading from 0 to 10 wt% show an incremental variation in trap centre and move towards the right. From Table 1, it is apparent that shallow traps around 0.8 eV are responsible for the lower mean time (faster decay), whereas deep traps around 0.87 eV are accountable for higher mean time (slower decaying).

The right shift in the trap centre is intuitively thought as broadening of trap depth and it can be correlated with the decrement in the decay rate of potential decay. Hence, the addition of filler up to 10 wt% broadens the trap depth and thereby prevents the charge transport through the bulk. Further increase in filler concentration leads to enhancement in surface and bulk conductivity which may bridge the material through charge transport.

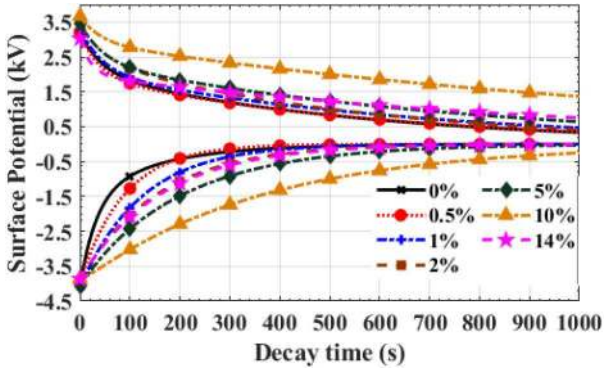


**Fig. 9** *Surface decay potential plot for +DC and –DC*

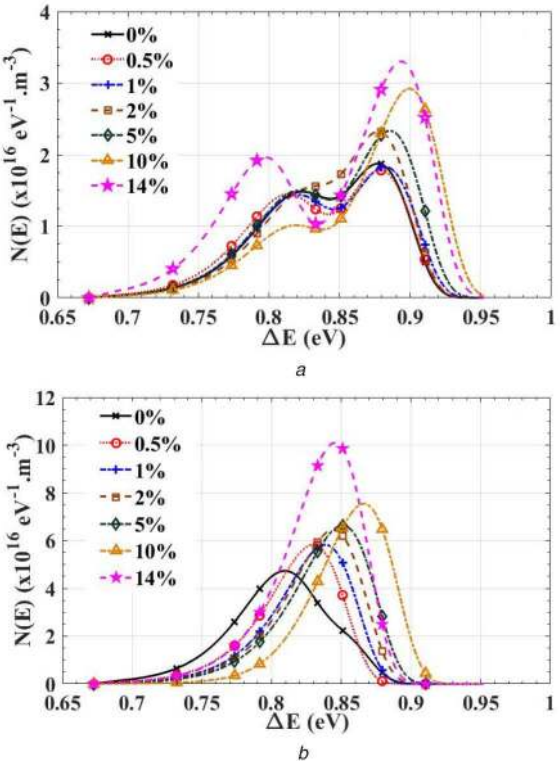


**Fig. 10** *Trap energy density versus trap depth plot for* ***(a)*** +DC input, ***(b)*** –DC input profile

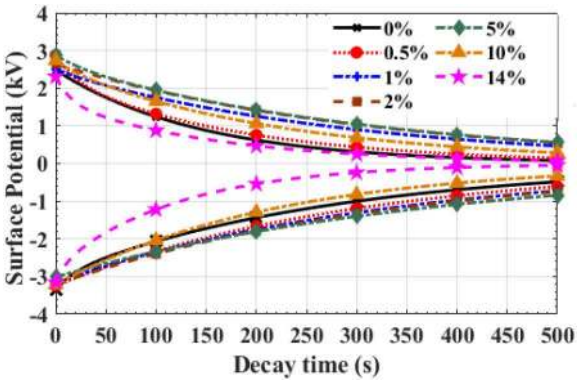


**Fig. 11** *Surface decay potential characteristics for lightning impulse input*

*3.1.4 Surface potential decay characteristics under lightning impulse voltage:* The variation in potential decay characteristics after injection of charges with the standard lightning impulse voltage is shown in Fig. 11.

It is observed that the potential decay under negative polarity is higher than positive polarity. The cause for it could be due to the fact that detraping is rapid with negative charges than the positive charges [21, 22]. The mean lifetime and trap depth of epoxy nanocomposites for different filler concentration are shown in Table 2.

**Table 1** Mean lifetime and trap centres of samples under DC

| Polarity | Positive DC | | Negative DC | |
|---|---|---|---|---|
| Sample, wt % | Mean lifetime ($\tau$) | Trap depth, eV | Mean lifetime ($\tau$) | Trap depth, eV |
| 0 | 387.9 | 0.9 | 61.7 | 0.8 |
| 0.5 | 403.7 | 0.9 | 90.0 | 0.8 |
| 1 | 440.7 | 0.9 | 123.8 | 0.8 |
| 2 | 427.2 | 0.9 | 156.1 | 0.8 |
| 5 | 529.9 | 0.9 | 194.1 | 0.9 |
| 10 | 988.1 | 0.9 | 398.1 | 0.9 |
| 14 | 758.7 | 0.9 | 167.2 | 0.8 |

**Table 2** Mean lifetime and trap centres of samples under lightning impulse

| Polarity | Positive polarity | | Negative polarity | |
|---|---|---|---|---|
| Sample, wt % | Mean lifetime ($\tau$) | Trap depth, eV | Mean lifetime ($\tau$) | Trap depth, eV |
| 0 | 144.7 | 0.8 | 276.4 | 0.9 |
| 0.5 | 180.7 | 0.8 | 299.8 | 0.9 |
| 1 | 300.8 | 0.9 | 339.3 | 0.9 |
| 2 | 318.8 | 0.9 | 342.0 | 0.9 |
| 5 | 322.8 | 0.9 | 391.7 | 0.9 |
| 10 | 228.3 | 0.9 | 219.9 | 0.9 |
| 14 | 160.1 | 0.8 | 123.2 | 0.8 |

With the decay process being found rapid in the case of lightning impulse voltage, further decay characteristics are fitted into the first-order exponential curve which eliminates the formation of the initial peak in energy density distribution plot, as shown in Figs. 12*a* and *b*.

The right shift in trap centres till 5 wt% reveals the formation of deep traps beyond which left shift in trap centres occurs where the potential decay is prominently due to shallow traps. The results are correlated with the potential decay characteristics observed under applied lightning impulse voltages, as shown in Fig. 11.

*3.1.5 Dielectric relaxation spectroscopy:* In general, the dielectric properties of material depend on atomic orientation and interfacial polarisation. The addition of filler induces polarisation (alignment of dipoles) process for an applied electric field. Fig. 13 shows the variation in permittivity of the epoxy nanocomposite material with different weight percentages of nanofillers in it. It is observed that the permittivity $\epsilon'$ increases with the increase in filler concentration [23]. Further, the maximum dielectric constant is observed for 14 wt% sample. Further, Paul *et al.* have investigated the electric energy density from permittivity and breakdown strength of the nanocomposites [23]. The conductive filler particle and surrounded dielectric epoxy matrix act as a tiny capacitor [8]. In the process, delocalisation of electrons from the outer shell makes the electrons to move freely under the applied electric field, and at the same time the capacitor network starts accumulating the charges and thereby increases the polarisability of the material, and subsequently increases the overall dielectric constant of the material [1].

Thus, with an increase in filler concentration in epoxy nanocomposites results in a decrease in packing density and interparticle distance. Furthermore, it increases the charge accumulation under an applied electric field which yields improved polarisability, leading to the increment in dielectric constant and at the same time capacitor with the addition of filler loading. On the other hand, the decrease in dielectric constant can be observed with respect to frequency, due to the decrease in the polarisability of dipoles. The orientation of dipoles is easier at lower frequencies in the direction of alternating electric field, causing improved polarisation subsequently leading to the higher value of dielectric

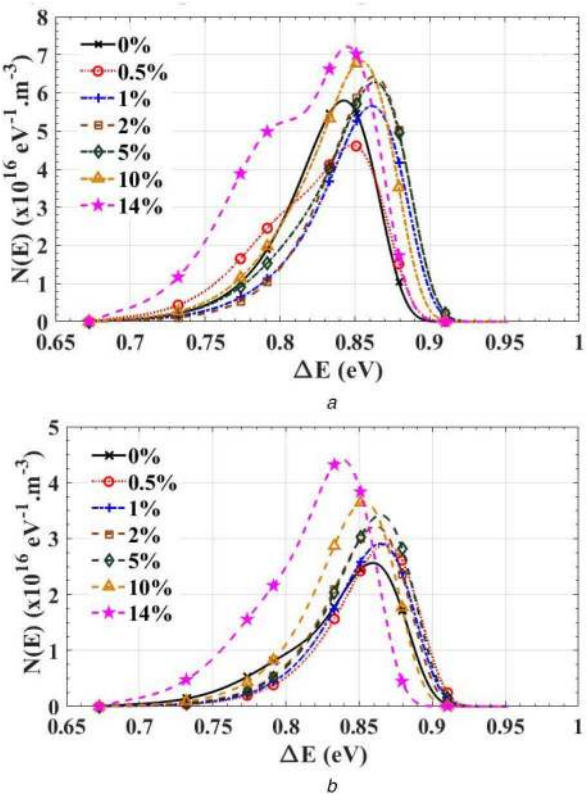


**Fig. 12** *Trap energy density versus trap depth plot for*
***(a)*** Positive polarity, ***(b)*** Negative polarity of a lightning impulse input

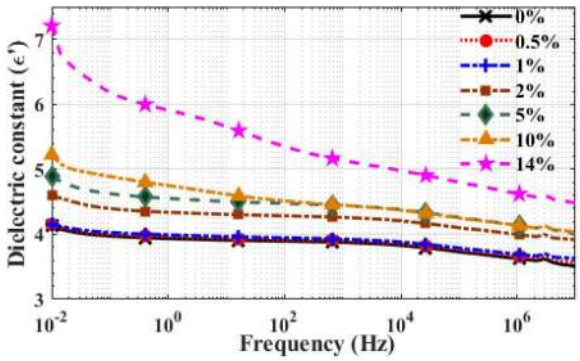


**Fig. 13** *Variation of the dielectric constant of Al–epoxy nanocomposites as a function of frequency*

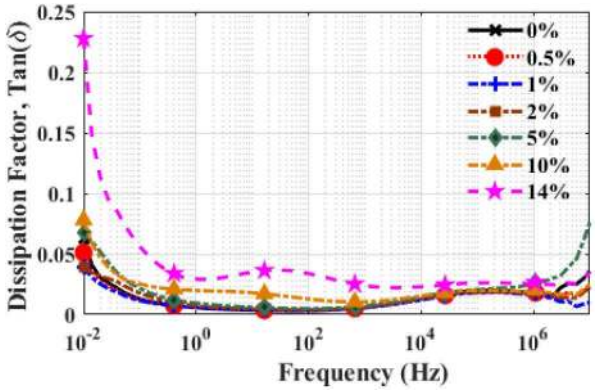


**Fig. 14** *Variation of the dissipation factor of nanocomposites as a function of frequency*

constant. Whereas diploes may not align for a higher rate of alternating electric field which cause a decrease in the polarisability and hence the reduced dielectric constant can be observed at higher frequencies.

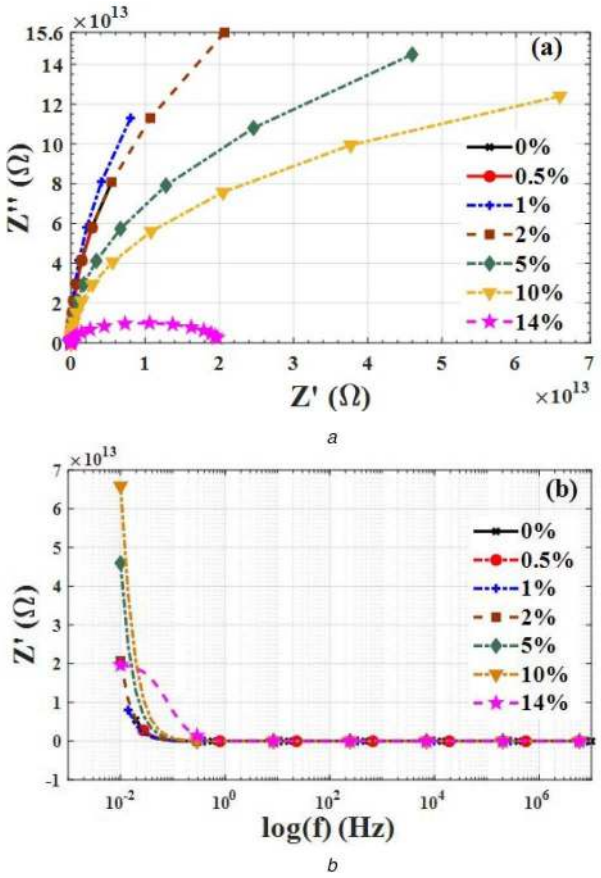


**Fig. 15** *Impedance spectroscopy with*
***(a)*** Nyquist plot for complex impedance ($Z'$ versus $Z''$), ***(b)*** Variation of $Z'$ with respect to frequency as a function of filler concentration

The conductive path created by the nanofillers allows the leakage current to flow and causes the portion of electrical energy to lose in the form of heat. As filler loading is increased, the conductive path formation becomes more which entails more leakage of current flow and more loss of thermal energy. Hence, the lower value of tan $\delta$ is desired for energy storage applications. From Fig. 14, decremented values of tan $\delta$ up to 2 wt% and incremented behaviour from 5 to 14 wt% can be observed. Although the increment in tan $\delta$ was found to be 5–10 wt%, they are in comparable limits of epoxy [8].

As proposed in the percolation theory, the overlapping of nanofillers nearing percolation limit bridges the dielectric network and thereby creates the conducting path through the material, which eventually leads to the increase in the conductivity of the sample. To validate this consistency, the impedance spectroscopy was employed to investigate bulk electrical properties and conductivity of samples. The Nyquist plot has been drawn between $Z'$ and $Z''$ as a function of filler loading and it is shown in Fig. 15*a*.

It is observed that the peak maxima of curves are reduced and the curve bends towards the $Z'$-axis with an increase in the filler concentration. It shows the reduction in overall impedance and more feasibility for the formation of conductive paths within the material at higher filler concentration. The variation in depressed semi-circular arc depicted in the Nyquist plot yields the variation of conductivity over the different filler concentration. Transformation of depressed semi-circular to semi-circular nature with the addition of filler is an indication of increased conductivity, which is in accordance with the proposed percolation theory [24]. Fig. 15*b* shows the variation of $Z'$ with respect to frequency over different filler concentrations. It is observed that the $Z'$ decreases with an increase in the frequency and almost negligible at higher frequencies. This behaviour can be attributed to space–charge polarisation which has predominant nature at low frequencies [25].

Further, the bulk resistance ($R$) and capacitance ($C$) of samples were determined by fitting the data to an equivalent parallel RC circuit. The Levenberg–Marquardt least-squares algorithm was

**Table 3** Fitted RC parallel circuit parameters for various filler concentrations

| Sample, wt% | Circuit parameters | | Electrical conductivity, $\sigma$ ($\times 10^{-12}$), S/m |
|---|---|---|---|
| | $R$ ($\times 10^{12}$), Ω | $C$ ($\times 10^{-12}$), F | |
| 0 | 1200.0 | 0.1 | 295.4 |
| 0.5 | 1600.0 | 0.1 | 299.4 |
| 1 | 1500.0 | 0.1 | 302.2 |
| 2 | 1200.0 | 0.1 | 360.8 |
| 5 | 500.0 | 0.1 | 457.3 |
| 10 | 300.0 | 0.1 | 905.4 |
| 14 | 30.0 | 0.1 | 2759.0 |

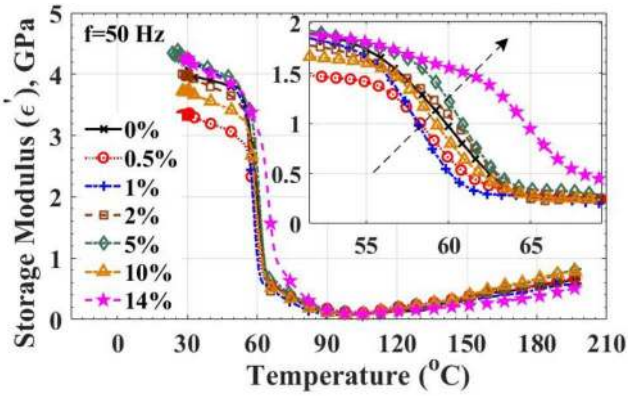


**Fig. 16** *Variation of storage modulus of Al–epoxy nanocomposites with different filler concentrations (f = 50 Hz)*

**Table 4** Glass transition temperature and activation energy values for different filler concentration

| Sample, wt % | $f$ = 1 Hz | $f$ = 10 Hz | $f$ = 25 Hz | $f$ = 50 Hz | Activation energy, eV | tan $\delta$ |
|---|---|---|---|---|---|---|
| 0 | 66.8 | 79.0 | 84.5 | 95.4 | 1.5 | 0.81 |
| 0.5 | 67.6 | 78.2 | 85.2 | 95.3 | 1.5 | 0.73 |
| 1 | 65.0 | 74.0 | 78.0 | 81.9 | 2.4 | 0.73 |
| 2 | 66.7 | 75.0 | 79.8 | 82.9 | 2.5 | 0.72 |
| 5 | 68.7 | 76.8 | 81.7 | 84.8 | 2.5 | 0.73 |
| 10 | 67.9 | 75.2 | 79.1 | 84.6 | 2.5 | 0.79 |
| 14 | 71.8 | 78.9 | 86.0 | 87.1 | 2.5 | 0.71 |

used for curve fitting and evaluating the circuit parameters. Table 3 provides circuit parameters viz. $R$ and $C$ as a function of filler concentration. It has been observed that the bulk resistance of samples has reduced at higher concentration of filler which can again be attributed to enhanced conductivity at higher concentrations of filler.

The variation in electrical conductivity of epoxy nanocomposites determined through DRS spectroscopy is shown in Table 3. The addition of metallic nanofiller to epoxy matrix shows a marginal increase in the conductivity up to 10 wt% and above which a drastic increase in conductivity is observed. This indicates that the material below percolation threshold behaves like a dielectric material, where the optimised inter-filler distance avoids the formation of a conductive path.

### 3.2 Dynamic mechanical analysis

Fig. 16 gives the variation of $\epsilon'$ for various filler concentrations at a frequency of 50 Hz.

The predominant viscoelastic properties such as storage modulus ($\epsilon'$), loss modulus ($\epsilon''$) and mechanical tan $\delta$ were recorded over different frequency and temperature ranges for all samples under consideration. The improved crosslink polymer chain density with an increase in the filler percentage has shown an increase in the storage modulus. For a given sample, it is observed

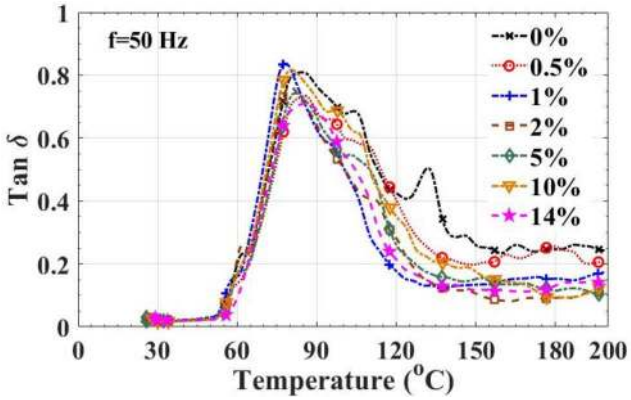


**Fig. 17** *Variation of tan δ with respect to filler concentration (f = 50 Hz)*

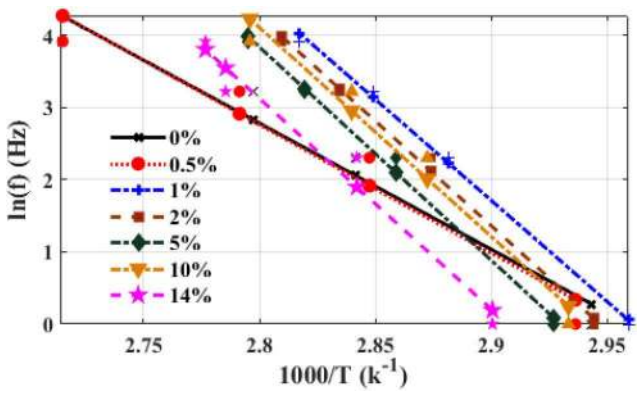


**Fig. 18** *Activation energy plot for Al–epoxy nanocomposites*

from Table 4 that the right shift in $\epsilon'$ curves in the transition region over increased values of frequencies gives the indirect indication of increment in the glass transition temperature $T_g$ [26].

The relaxation peak observed for the samples under consideration exists in the temperature range from 80 to 90°C. The variation in tan $\delta$ with increasing concentration of filler at 50 Hz frequency is shown in Fig. 17. It is found that the tan $\delta$ value is decreasing at the glass transition temperature on the addition of nanoparticles and the corresponding values are provided in Table 4.

For a material, it is possible to calculate the activation energy ($E_a$) at which the maximum degradation occurs through the data from Table 4 using the Arrhenius equation

$$f = f_0 * e^{(-E_a/RT)} \quad (6)$$

where $f'$ is the test frequency, $f_0$ is a constant, $T$ is the temperature (K) and $R$ is the universal gas constant. The slope from the graph shown in Fig. 18 between 1000/$T$ and log($f$) gives the activation energy, and the calculated values of $E_a$ are presented in Table 4. It is observed that upon reinforcing the filler to the epoxy matrix, the activation energy is increased for the sample with 2 wt% and stays almost constant beyond the addition of filler concentration [27].

### 3.3 LIBS and hardness test

The laser-induced emission spectra of epoxy nanocomposites with different weight percentages of nanofillers are shown in Fig. 19.

Laser ablation of the material causes the plasma to generate and emit spectra consisting of intensities of constituent elements present in the material [22]. NIST database was used to match the distinct peaks in spectra at their respective wavelengths. The spectra shown in Fig. 19 consist of not only Al peaks but also the other components viz. C, H, N and O. It can be attributed to the functional groups present in the epoxy and hardener. Intensities of persistent Al peaks of same phase present at wavelengths of 308.2 and 396.1 nm were used to calculate the plasma temperature and electron density of the plume formed due to laser shine.

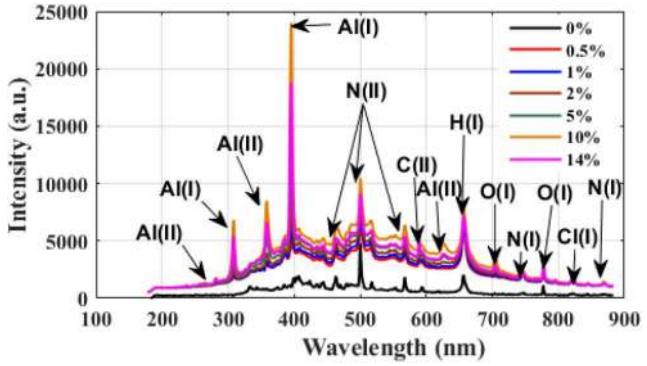


**Fig. 19** *Laser-induced breakdown spectra of Al–epoxy nanocomposites*

**Table 5** Plasma temperature, electron density and Vickers hardness values of nanocomposites with respect to filler concentration

| Sample, wt % | Plasma temperature, K | Electron density ( × $10^{16}$) | Hardness ( × HV0.1) |
|---|---|---|---|
| 0 | 4614.2 | 0.2 | 20.1 |
| 0.5 | 5712.8 | 4.4 | 20.8 |
| 1 | 6640.9 | 24.2 | 21.8 |
| 2 | 7894.3 | 127.3 | 21.6 |
| 5 | 10,046.0 | 838.3 | 21.9 |
| 10 | 10,064.0 | 848.7 | 24.3 |
| 14 | 9773.3 | 691.2 | 23.3 |

Boltzmann–Saha equation can be used to calculate the plasma temperature ($T_e$) considering local thermal equilibrium conditions, and is given by [28]

$$T_e = 1.44 \times \frac{E_2 - E_1}{\ln[l_1\lambda_1 A_2 g_2 / l_2\lambda_2 A_1 g_1]} \quad (7)$$

Here $g_1$ and $g_2$ are the statistical weights of excited energy levels $E_1$ and $E_2$, respectively, $A_1$ and $A_2$ are the transition probabilities of states, $I_1$ and $I_2$ are the intensities of corresponding elemental peaks at $\lambda_1$ and $\lambda_2$ wavelengths, respectively. Similarly, the electron density ($n_e$) could be estimated at the time of plasma irradiation by governing the modified Saha equation [28], i.e.

$$n_e = 6.6 \times 10^{21} \times \frac{I_1}{I_2}\frac{A_2 g_2}{A_1 g_1} \times \exp\left[-\frac{E_{ion} + E_2 - E_1}{kT_e}\right] \quad (8)$$

where $E_{ion}$ is the first ionisation potential of isolated neutral gaseous aluminium atom (5.986 eV) and $k$ is the Boltzmann constant.

The plasma temperature, electron density and Vickers hardness values of nanocomposites with the variation of filler concentration are presented in Table 5, which indicate that the plasma temperature enhancement occurs when the hardness of the material is high.

## 4 Conclusions

The important conclusions arrived based on the present study are the following:

- Optimised quantity of self-passivated nanoaluminium filler mixed with epoxy resin to acquire enhanced mechanical and dielectric properties of nanocomposites was fabricated.
- Variation in contact angle and surface roughness is not significant with an increase in filler content in epoxy nanocomposite but drastic reduction in the contact angle is observed on corona ageing of the specimen. Water droplet initiated CIV is high under negative DC voltage followed with positive DC and AC voltages. With corona-aged specimen, the similar characteristics are observed with a reduction in CIV under AC and DC voltages.
- The bandwidth of the UHF signal generated due to water droplet initiated corona discharge lies in the range of 0.5–1.2 GHz.
- Surface potential decay studies were carried out by injecting charges by DC/lightning impulse voltage corona activity and it revealed the initial fast potential decay and subsequently the slower potential decay. Based on trap energy density versus trap depth plot, it is evident that shallow traps occur at around 0.8 eV and deep traps formed at around 0.87 eV.
- The dielectric permittivity, conductivity and loss factor have increased with an increase in the filler content in epoxy–aluminium nanocomposites. The Nyquist plot obtained clearly indicates the increase in conductivity with the filler content. The bulk resistance ($R$) and capacitance ($C$) of samples were determined through the Levenberg–Marquardt algorithm for obtaining the equivalent parallel RC circuit model.
- DMA studies clearly indicate that the incorporation of nanofillers increases the glass transition temperature and reduces the mechanical tan $\delta$ over increased values of frequencies. An improvement in activation energy was observed until 2 wt% and it remains constant beyond the addition of filler concentration.
- A direct linear correlation is observed between the plasma temperature measured through LIBS spectra and hardness of the material.

## 5 Acknowledgment

The author (R.S.) wishes to thank the Department of Science and Technology, New Delhi for sponsoring the project (DST/NM/NT/2018/33(c)) on transformer insulants.

## 6 References

[1] Wang, Z., Zhou, W., Sui, X., *et al.*: 'Enhanced dielectric properties and thermal conductivity of Al/CNTs / PVDF ternary composites', *J. Reinf. Plast. Compos.*, 2015, **34**, (14), pp. 1126–1135
[2] Huang, X.Y., Jiang, P.K., Kim, C.U.: 'Electrical properties of polyethylene/aluminum nanocomposites', *J. Appl. Phys.*, 2007, **102**, (12), p. 124103
[3] Zhou, W., Yu, D.: 'Thermal and dielectric properties of the aluminum particle / epoxy resin composites', *J. Appl. Polym. Sci.*, 2010, **118**, (6), pp. 3156–3166
[4] Lu, J., Wong, C.P.: 'Recent advances in high-k nanocomposite materials for embedded capacitor applications', *IEEE Trans. Dielectr. Electr. Insul.*, 2008, **15**, (5), pp. 1322–1328
[5] Paul, S., Sindhu, T.K.: 'Effect of filler particle size on electric energy density of epoxy-aluminum nanocomposites', *IEEE Trans. Dielectr. Electr. Insul.*, 2016, **23**, (5), pp. 2786–2794
[6] Zhou, W., Yu, D.: 'Fabrication, thermal, and dielectric properties of self-passivated Al/epoxy nanocomposites', *J. Mater. Sci.*, 2013, **48**, (22), pp. 7960–7968
[7] Elanseralathan, K., Karthick, V., Kumar, R.S.D., *et al.*: 'Effect of filler concentration on the breakdown strength of epoxy nanocomposites'. 2017 6th Int. Conf. on Computer Applications in Electrical Engineering – Recent Advances (CERA), Roorkee, India, 2017, pp. 226–229
[8] Paul, S., Sindhu, T.: 'Development of epoxy-aluminum nanocomposite dielectric material with low filler concentration for embedded capacitor applications', *IEEE Trans. Dielectr. Electr. Insul.*, 2014, **21**, (2), pp. 460–466
[9] Singha, S., Thomas, M.J.: 'Dielectric properties of epoxy nanocomposites', *IEEE Trans. Dielectr. Electr. Insul.*, 2008, **15**, (1), pp. 12–23
[10] Xu, J., Moon, K.S., Tison, C., *et al.*: 'A novel aluminum-filled composite dielectric for embedded passive applications', *IEEE Trans. Adv. Packag.*, 2006, **29**, (2), pp. 295–306
[11] Shahravan, A., Desai, T., Matsoukas, T.: 'Passivation of aluminum nanoparticles by plasma-enhanced chemical vapor deposition for energetic nanomaterials', *ACS Appl. Mater. Interfaces*, 2014, **6**, (10), pp. 7942–7947
[12] Tanaka, T., Kozako, M., Fuse, N., *et al.*: 'Proposal of a multi-core model for polymer nanocomposite dielectrics', *IEEE Trans. Dielectr. Electr. Insul.*, 2005, **12**, (4), pp. 669–681
[13] Molinié, P.: 'Measuring and modeling transient insulator response to charging: the contribution of surface potential studies', *IEEE Trans. Dielectr. Electr. Insul.*, 2005, **12**, (5), pp. 939–950
[14] Gao, Y., Wang, J., Liu, F., *et al.*: 'Surface potential decay of negative corona charged epoxy/$Al_2O_3$ nanocomposites degraded by 7.5-MeV electron beam', *IEEE Trans. Plasma Sci.*, 2018, **46**, (7), pp. 2721–2729
[15] Du, B.X., Jiang, J.P., Zhang, J.G., *et al.*: 'Dynamic behavior of surface charge on double-layer oil–paper insulation under pulse voltage', *IEEE Trans. Dielectr. Electr. Insul.*, 2016, **23**, (5), pp. 2712–2719
[16] Sarathi, R., Animesh, S., Chen, Y., *et al.*: 'Understanding surface discharge activity with epoxy silicon carbide nanocomposites', *Polym. Eng. Sci.*, 2017, **57**, (12), pp. 1349–1355

[17] Sarathi, R., Mishra, P., Gautam, R., *et al.*: 'Understanding the influence of water droplet initiated discharges on damage caused to corona-aged silicone rubber', *IEEE Trans. Dielectr. Electr. Insul.*, 2017, **24**, (4), pp. 2421–2431
[18] Tanaka, T., Imai, T.: '*Advanced nanodielectrics: fundamentals and applications*' (CRC Press, Singapore, 2017, 1st edn.)
[19] Moreno, V.M., Gorur, R.S., Kroese, A.: 'Impact of corona on the long-term performance of nonceramic insulators', *IEEE Trans. Dielectr. Electr. Insul.*, 2003, **10**, (1), pp. 80–95
[20] Phillips, A.J., Childs, D.J., Schneider, H.M.: 'Aging of non-ceramic insulators due to corona from water drops', *IEEE Trans. Power Deliv.*, 1999, **14**, (3), pp. 1081–1086
[21] Du, B.X., Li, J., Du, W., *et al.*: 'Dynamic behavior of surface charge on direct-fluorinated polyimide films'. Proc. of IEEE Int. Conf. on Solid Dielectrics, ICSD, Bologna, Italy, 2013, pp. 329–332
[22] Desai, B.M.A., Mishra, P., Vasa, N.J., *et al.*: 'Understanding the performance of corona aged epoxy nano micro composites', *Micro Nano Lett.*., 2018, **13**, (9), pp. 1280–1285
[23] Paul, S., Sindhu, T.K.: 'Synthesis and characterization of epoxy-aluminum nanocomposites for energy storage applications', *IEEE Trans. Dielectr. Electr. Insul.*, 2014, **21**, (5), pp. 2164–2217
[24] Thakur, S., Rai, R., Bdikin, I., *et al.*: 'Impedance and modulus spectroscopy characterization of Tb modified $Bi_{0.8}A_{0.1}Pb_{0.1}Fe_{0.9}Ti_{0.1}O_3$ ceramics', *Mater. Res.*, 2016, **19**, (1), pp. 1–8
[25] Mandal, S.K., Singh, S., Dey, P., *et al.*: 'Frequency and temperature dependence of dielectric and electrical properties of $TFe_2O_4$ (T = Ni, Zn, $Zn_{0.5}$ $Ni_{0.5}$) ferrite nanocrystals', *J. Alloys Compd.*, 2016, **656**, pp. 887–896
[26] Olowojoba, G.B., Kopsidas, S., Eslava, S., *et al.*: 'A facile way to produce epoxy nanocomposites having excellent thermal conductivity with low contents of reduced graphene oxide', *J. Mater. Sci.*, 2017, **52**, (12), pp. 7323–7344
[27] Sarathi, R., Sahu, R.K., Kumar, P.R., *et al.*: 'Understanding the performance of epoxy nano composites – a physico-chemical approach', *IEEJ Trans. Fundam. Mater.*, 2006, **126**, (11), pp. 1112–1120
[28] Djilianova, O., Sadowski, M.J., Skladnik-Sadowska, E.: 'The Cu spectra as a tool for late plasma focus diagnostics', *J. Phys. Conf. Ser.*, 2006, **44**, (1), pp. 175–178